Structural Characterization, Electrical Transport Properties and Gamma-Ray Shielding- Parameters of Some Phosphate Glasses Containing By-Pass Cement Dust

A.G. Mostafa [1]*, S.M. Salem[1], O.M. Yassin[1], R.A. Abu Gasser[1] and K.H. Idress[2]

[1.] Phys. Dept., Faculty of Science, Al-Azhar University, Nasr City, Cairo, Egypt
[2.] Phys. Dept., Faculty of Science, Sert University, Libya
*drahmedgamal.@yahoo.com

Abstract: Some phosphate glasses containing different amounts of by-pass cement dust have been prepared by the melt quenching method. The selected molecular composition was [(100-x) % P_2O_5 - (x) % By-Pass Cement Dust (where $30 \leq x \geq 60$)]. The obtained experimental density and molar volume values were inspected and were then compared with those obtained empirically for the close packed structure of the corresponding compounds. These comparisons evidenced the short-range order and randomness character of the studied samples. The electric and dielectric properties were thoroughly investigated. The appearance of maxima and minima in the total conductivity by pass cement dust concentration dependence can be attributed to the mixed alkali – alkaline earth effect (K_2O & CaO). The suitability of such glasses to act as gamma-ray shielding materials was also examined and a correlation between the chemical composition (By-Pass Cement Dust content) and gamma-ray attenuation behavior was established.

[Mostafa AG, Salem SM, Yassin OM, Abu Gasser RA and Idress KH. **Structural Characterization, Electrical Transport Properties and Gamma-Ray Shielding- Parameters of Some Phosphate Glasses Containing By-Pass Cement Dust.** *Nat Sci* 2018;16(2):114-123]. ISSN 1545-0740 (print); ISSN 2375-7167 (online). http://www.sciencepub.net/nature. 17. doi:10.7537/marsnsj160218.17.

Keywords: By-pass Cement Dust; Phosphate glasses; Electrical Transport Properties, Gamma–ray attenuation parameters

1. Introduction

Amorphous materials and glasses appear now of interest due to their important functional applications in both science and technology [1]. Many efforts have been devoted to study either high purity glasses used for scientific purposes or glasses doped with controlled amounts of environmental wastes used for commercial applications [2-3]. It is known also that the variation of the composition of a glass network affect directly the properties of such glass [4-6], and among all properties, electrical conductivity is of high interest. Although many research works have been done to investigate the electrical conductivity of such like glasses, more work are still needed to clarify the true conduction mechanism through glasses [5-7]. Also, the use of different radioactive isotopes in various daily life fields is spread now, and it is known that, for different nuclear radiation sources, special shielding materials are required [8-10]. Since glasses are usually transparent and can be easy manufactured, therefore, another interesting application can be checked, which is the γ-ray attenuation coefficient of the studied glasses.

From another point of view, by-bass cement dust (BCD), as an industrial waste, represents a dangerous by-product of cement industry and it accumulated in huge amounts in Egypt. It causes various diseases, especially those related to human respiratory system [11]. According to the chemical analysis, such waste consists of various oxides (mainly, CaO, SiO_2, Na_2O, K_2O and Fe_2O_3), where all these oxides can be used for manufacturing different types of oxide glass [12,13].

However, in this article, it will be tried to prepare some phosphate glasses with different additives of BCD, as high as possible, aiming to consume the waste accumulation as well as to obtain low coast glasses that can be used for different industrial and scientific applications. The prepared glasses will be thoroughly investigated from the structural and electrical properties points of view. Then their gamma-ray shielding parameters will be also studied in order to investigate whether they can be used as transparent γ-ray shields or as capsulations for the radio-active wastes before interment underground.

Table 1. The chemical composition of the used BCD

Constituent	**CaO**	**K_2O**	**SiO**	**Fe_2O_3**	**Al_2O_3**	**MgO**	**Na_2O**	*** LOI**
Amount%	**60.63**	**10.74**	**6.96**	**3.60**	**2.36**	**1.54**	**0.03**	**16.59**

* LOI is the loss of ignition

2. Experimental

BCD was supplied by Tora Cement Co., Helwan, Cairo, Egypt and it was chemically analyzed by using X-ray fluorescence (XRF) apparatus model PA Nalytical Axios advanced, Netherlands. The obtained chemical composition is exhibited in Table (1).

The selected glasses were prepared by weighting suitable amounts from ammonium di-hydrogen ortho-phosphate and the supplied BCD, so that when melted, they supply glasses having the following composition [(70-x) P_2O_5 - x BCD, where $30 \leq X \geq 60$ in steps of five. The batches were ground and mixed well in an agate mortar and they were then transferred into porcelain crucibles and the crucibles were inserted into an electric muffle furnace at RT. The temperature of the furnace was raised up to 1100ºC during one hour and left at this temperature for 2 hours. Melts were stirred several times during melting and were then poured between two copper plates in air. The obtained glass samples -just after solidifying- were transferred to the annealing furnace at 450ºC for 2 hours and the furnace was then turned off and left to cool to RT with a cooling rate of about 1.5ºC/min.

XRD patterns were obtained by using Rigaku-RINT 2100, outfitted with Cuk_α radiation of λ= 0.1541 nm and the operating current and voltage were 300 mA and 50 KV, respectively.

The experimental density (ρ_{exp}) was measured by applying Archimedes principle, using carbon tetra-chloride (CCl_4) as an immersion liquid. In such principle, a sample was weighted in air (M_a) and in CCl_4 (M_l), and then (ρ_{exp}) can be calculated by using equation (1) [14],

$$\rho_{exp} = \left[\frac{M_a}{M_a - M_l}\right] \rho_l \quad (1)$$

The experimental molar volume values $(V_m)_{exp}$ were then calculated using equation (2),

$$(V_m)_{exp} = \frac{M_m}{\rho_{exp}} \quad (2)$$

where M_m is the main molecular weight in (g/mol) of a glass sample.

The empirical density values (ρ_{emp}) were also calculated using the following relation [14],

$$\rho_{emp} = \sum_i \rho_i X_i \quad (3)$$

where ρ_i are the densities of the oxides forming a glass sample and X_i are the mole fractions of each oxide.

The empirical molar volume $(V_m)_{emp}$ values were then calculated using equation (2) with replacing ρ_{exp} by ρ_{emp} [14].

For electrical measurements, the obtained solid glasses were polished from both sides in order to obtain optically flat disk shape samples of 8 mm diameter and 1 mm thickness. The disks were then coated from both sides with an air-drying silver paste to achieve good electrical contact. The measurements were carried out by using a computerized Stanford LCR bridge model SR 720 at four fixed frequencies [0.12, 1, 10, 100 kHz]. All measurements were performed in the temperature range from RT up to 250ºC.

The gamma-ray attenuation parameters (total mass attenuation coefficient $(\mu_l/\rho)_{m\ (total)}$, half value layer (HVL) and Mean free path (MFP) of a glass sample were then calculated by applying WIN-XCOM program, based on the mixture rule [15].

3. Results and Discussion

3.1. Structural Characterization

Visually, all the obtained solid samples appeared to be transparent and free of inclusions and air bubbles, that is they appeared in good and hemogeneus glassy phase. But, in order to confirm the amorphous state of the studied samples, XRD analysis was applied. However, Fig. (1) shows the obtained XRD patterns of all glasses where it can be seen that all patterns exhibit no any sharp crystallization peaks, but only a hump at 2Θ between 20º & 30º degree. Therefore, these results showed that, all samples exhibit amorphous nature and short-range order character [16].

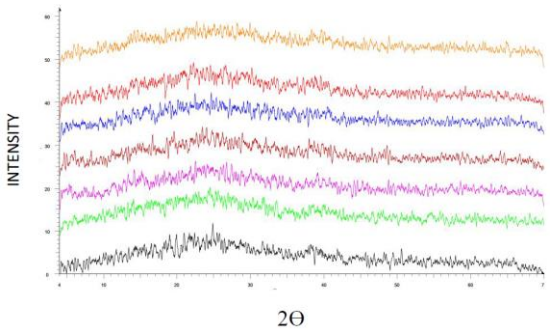

Figure 1. The obtained XRD patterns of the studied glasses

On the other hand, IR analysis was early known to be an effective tool to investigate the internal structure of various glasses and amorphous materials. Therefore, Fig. (2) shows the obtained IR spectra in the range from 400 to 4400 cm^{-1} for all samples.

The appeared broad bands, in all spectra refer to the homogeneity and amorphous nature of the studied glasses. But it appeared that, the range of interest is only between 400 and 2000 cm^{-1}. This range was undergoing to the de-convolution program in order to inspect, as really as possible, the IR bands in these spectra. However, Fig. (3) represents the de-

convoluted spectrum of the sample containing 60 mol % BCD, as representative spectrum.

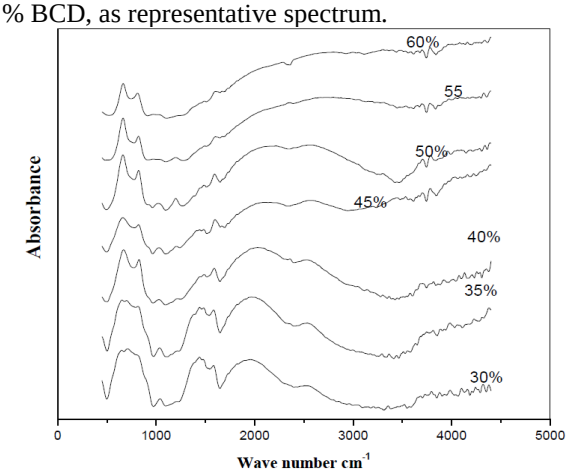

Figure 2. The obtained IR spectra of all the studied glasses

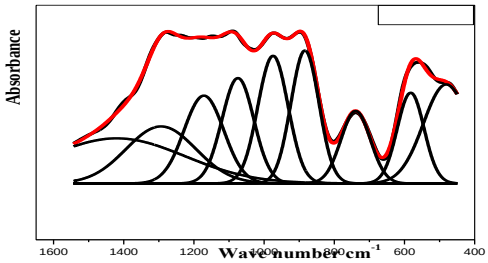

Figure 3. The de-convoluted IR spectrum of the sample containing 60 mol% BCD, as representative spectrum

The obtained real bands can be attributed to the vibration of some groups as well as some bond vibration in the glass networks and these bands can be interpreted as follows:

1- The band appeared at about 490 cm^{-1} in the spectra of all samples, can be assigned to the symmetric bending vibration of Si–O–Si in SiO_4 tetrahedra [17].

2- The band appeared in between 550 and 580 cm^{-1} can be assigned to P–O bond vibration in PO_4 tetrahedra [18].

3- The band appeared in the range from 735 to 760 cm^{-1}, in the spectra of all glasses can be attributed to the symmetric stretching vibration of P-O-P bond in Q^1 speeches [19].

4- The band appeared in between 890 and 910 cm^{-1}, can be assigned to the asymmetric stretching vibration of P-O-P bond in Q^1 speeches [20]. It is observed that these bonds shifted to higher frequencies, which can be attributed to some changes in phosphate chain length as well as some changes in P–O–P bond angles, since P–O–P bond angles depend on the characteristics of the metal cations in phosphate network [21].

5- The band appeared around 1055 cm^{-1}, can be assigned to the PO^3 vibration and/or the vibration of $(PO_4)^{3-}$ structural group in Q^o speeches [22].

6- The band appeared around 1140 cm^{-1} can be correlated to the vibration of two non- bridge oxygen atoms bonded to a single phosphorus atom in PO_2 unit (O-P-O) [23].

7- The band appeared in the range from 1215 to 1240 cm^{-1}, can be correlated to the symmetric stretching vibration of two non-bridge oxygen atoms bonded to a phosphorus atom in PO_2 unit (O-P-O) and / or the vibration O=P in Q^2 units [24].

8- The band appeared from 1280 to 1310 cm^{-1}, can be assigned to the asymmetric stretching vibration modes of non-bridging oxygen atom bonded to a phosphorus atom and/or the vibration of P=O bond in Q^2 speeches [25].

9- The band appeared in the range from 1410 to 1430 cm^{-1} can be assigned to the vibration of the present molecular water or hydroxyl-related bonds [26].

However, the IR results indicated that different structural phosphate and silicate groups appeared in the glass networks, and with the gradual increase of BCD, the intensities of silicate groups vibrations increased. The introduced CaO (the major constituent in the BCD) increases the non-bridge oxygen atoms and decreases H_2O and OH groups, which in turn act to strengthening the glass networks.

3.2. Density and Molar Volume

Both the obtained density values (ρ_{exp} & ρ_{emp}) are plotted in Fig. (4), for comparison as a function of BCD content. It is seen that both ρ_{exp} & ρ_{emp} increased gradually and linearly with the gradual increase of BCD, and the empirical density is usually higher than the corresponding experimental ones.

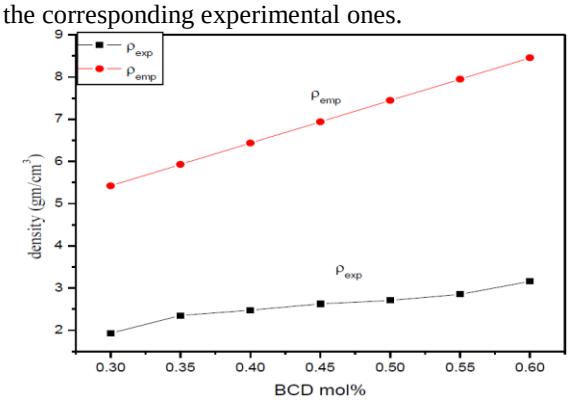

Figure 4. The variation of both density values (ρ_{exp} & ρ_{emp}) versus BCD content

Since the molar volume is directly related to the internal spatial structure of materials, it is suitable to

exhibit also the change of the molar volume as a function of BCD of the studied glasses. Both molar volume values ($V_{m\ emp}$ & $V_{m\ exp}$) are exhibited in Fig. (5), as a function of BCD.

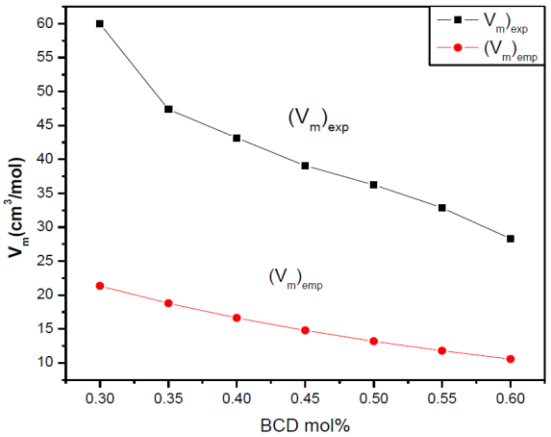

Figure 5. The variation of both molar volume values ($V_{m\ emp}$ & $V_{m\ exp}$) versus BCD content

It is observed that both values show gradual linear decrease and the empirical values are usually lower than those obtained experimentally.

The observed variations of both density and molar volume values may be due to the introduced BCD which contains various positive cations. These cations fill mostly the network vacancies, and in turn decrease the internal free volume.

Accordingly, the density is logically increased while the molar volume decreased. In addition, it can be stated that, the higher empirical density as well as the lower empirical molar volume in comparison to the corresponding experimental values can be taken as evidences for the amorphous nature and the short-range order character of the studied samples [27].

3.3. Electrical Transport Properties

It is known that the frequency dependence total conductivity (σ_T) for all amorphous materials and glasses follows the exponent law of equation (4),

$$\sigma_T = \sigma_{dc} + A\omega_s \quad (4)$$

where σ_{dc} is the frequency independent conductivity, A is a weakly temperature dependent factor, ω is the angular frequency and s is the exponent factor (usually less than or equal to unity) [28-29]. The values of the total conductivity temperature dependence for the sample containing 45 mol% BCD are exhibited in Fig. (6), as a representative figure, and all samples exhibit approximately similar behavior.

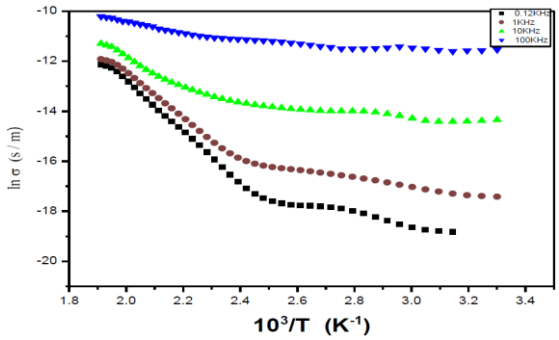

Figure 6. The total conductivity (σ_T) temperature dependence, for the sample containing 45 mol% BCD, as representative figure

At relatively low temperatures the conductivity shows weak temperature dependence and strong frequency dispersion, while at relatively high temperatures, it shows strong temperature dependence and weak frequency dependence. It is seen that; the dc conductivity is dominant at high temperatures while the ac conductivity is dominant at low temperatures. It can be concluded, from the conductivity values, that all samples behave like semiconductors [30].

Fig. (7), shows the variation of ln σ_T as a function of BCD, where two maxima and two minima are easily observed.

It is expected usually that, glasses exhibit roughly linear behavior with changing their chemical composition. But glasses containing two different alkali oxides represent a major exception to this trend due to the interaction between the co-presence of two different alkali ions or the co-presence of an alkali and an alkaline earth cation. Such behavior is known usually as mixed alkali effect (MAE) or mixed alkali-alkaline earth effect (MAAE) [31].

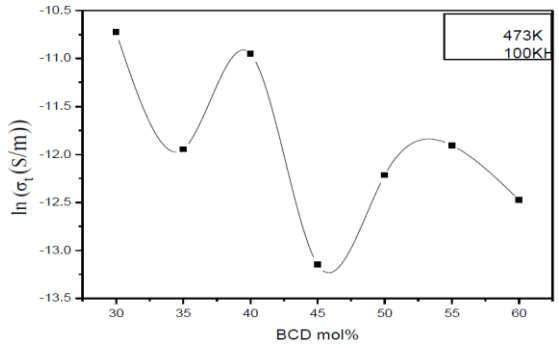

Figure 7. The variation of the total conductivity as a function of BCD

Since the used BCD consists of 60.4% CaO, and 10.7% K_2O, it is supposed that an electrical resistance appeared due to the interaction between the present alkali (K^+) and alkaline earth (Ca^{2+}) cations at certain compositions. Similar behavior has been previously

observed when the electrical conductivity of various ionic conductive glasses has been studied [32].

The deviation from linearity appeared so great that two maxima (at 40 and 55 mol%) and two minima (at 35 and 45) are easily observed. That is the influence of the co-presence of CaO and K_2O was observed as a dramatic non-linear trend due to the interaction between K^+ and Ca^{2+} cations, where the resistance increased with increasing the difference between the ionic radii of both the present alkali and alkaline earth cations [31, 32]. The concentrations of both CaO and K_2O present in BCD for all samples were calculated and exhibited in Table (2).

Table 2. The concentrations of CaO & K_2O in all the prepared samples

BCD mol %	30	35	40	45	50	55	60
CaO Mol %	18	21	24	27	30	33	36
K_2O Mol %	3.36	3.85	4.4	4.95	5.5	6.05	6.6

From this Table, it appeared that, large amounts of both CaO and K_2O are dissoluted and co-present in all samples. However, it can be supposed that, the mixed alkali-alkaline earth effect represents an effective factor that affect the total conductivity of the studied glasses.

The relation between ln (σ_T) and ln (ω), at a fixed temperature (325 K), for the sample containing 45 mol% BCD is exhibited in Fig. (8), as a representative figure, and all samples exhibit approximately similar behavior.

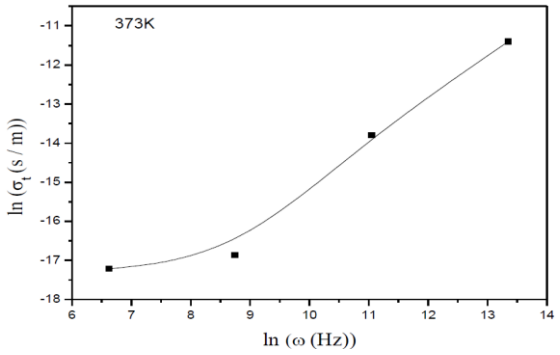

Figure 8. The variation of (ln σ_T) versus (ln (ω)) at a fixed temperate (325 K), for the sample containing 45 mol% BCD, as representative curve

Dotes and solid line represent the experimental data and theoretical fitting respectively. It can be seen that, at low frequencies the conductivity is approximately stable and is independent on frequency, while at high frequencies the conductivity shows gradual linier increase [33]. According to all the obtained data, it can be stated that all samples show semiconducting behavior.

The dc conductivity values were then calculated from the fitting of the experimentally obtained σ_T data with equation (4) and the obtained data are then plotted in Fig. (9) as a function of BCD content.

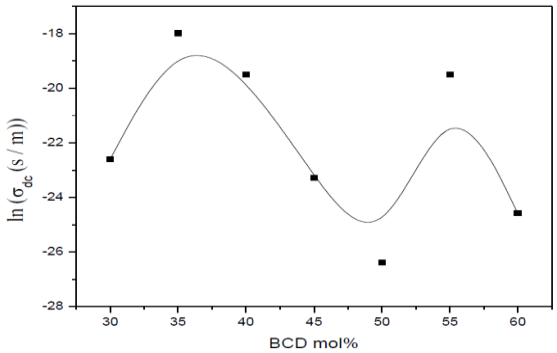

Figure 9. The variation of σ_{dc} as a function of BCD

It is seen that the variation of σ_{dc} is a non-linear behavior also and a maxima and a minima are exhibited at 35 and 55 mol% BCD, corresponding to CaO concentrations of 21 and 33 mol% respectively and the amounts of K_2O are also 3.3 and 6.05 mol% respectively. It can be supposed that the observed non-linear behavior may be due to the mixed alkali-alkaline earth effect [31, 32].

The dc electrical activation energy (ΔE) can be then calculated form the slopes of the obtained straight lines of the studied sample at relatively high temperatures (where the dc conductivity is dominant), according to Arhenius equation (equation 5),

$$\delta_{dc} = \sigma_0 \exp(-\Delta E/kT) \quad (5)$$

where σ_0 is the pre-exponential factor, ΔE is the activation energy, k is Boltzmann constant and T is the absolute temperature. The variation of the activation energy with BCD is exhibited in Fig. (10), where this variation shows approximately the reverse behavior of the dc conductivity [31, 32] and such trend was expected to be logic.

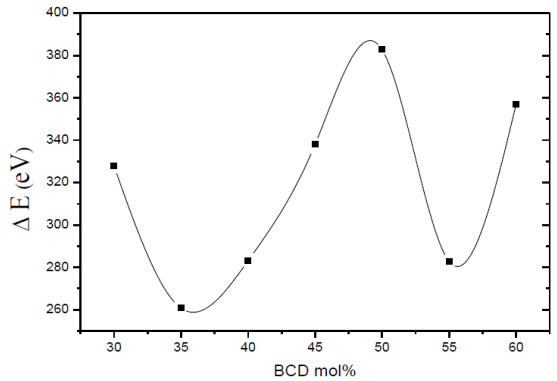

Figure 10. The variation of ΔE values as a function of BCD

The understanding of the microscopic transport mechanism for conduction in glass is a longstanding problem in glass science. Therefore, it was now checked in the studied samples. Fig. (11), shows the variation of the S-factor as a function of temperature for the sample containing 45 mol% BCD as representative figure, and all samples show approximately similar behavior.

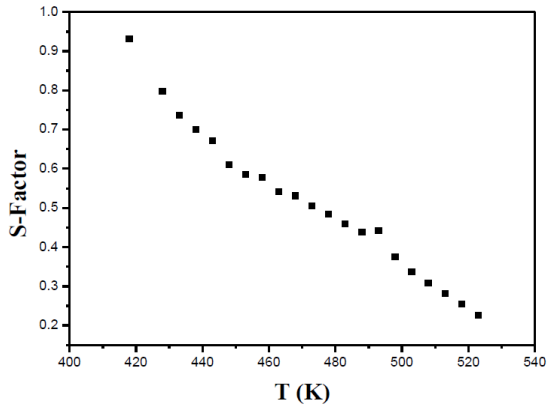

Figure 11. The variation of the S- factor as a function of temperature for the sample containing 45 mol% BCD, as representative figure

From this figure, it is observed that S decreased gradually with temperature, which was found in complete agreement with equation (6) that represents the behavior of the correlated barrier hoping (CBH|) mechanism.

Because of such agreement between the experimental behavior of the S and those predicted by Elliot [30], it can be supposed that such model can be used to describe the conduction mechanism in these glasses, and it is observed that, all samples exhibit similar behavior.

$$S = 1 - \frac{6KT}{W_m - KT\ln(\omega\tau_0)} \quad (6)$$

where ($\tau_0 = f_0^{-1}$) is the characteristic relaxation time in between 10^{-9} and 10^{-12} sec, k is Boltzmann constant, T is the absolute temperature and Wm is the energy required to remove an electron from its site to infinity. However, it can be supposed that, the conduction mechanism follow the CBH model in all the studied glasses [30].

The dielectric constant (ε') has been also measured, and Fig. (12) Shows the variation of ε' as a function of temperature for the sample containing 45 mol% BCD, as representative figure and all samples exhibit similar behavior.

It is observed that at low temperatures, ε' is almost independent on temperature and frequency, while at high temperatures it increases gradually as the temperature was increased, but it shows an inverse variation with frequency. The reason for this behavior is that, the electric dipoles move almost parallel to the external electric field and create an inverse internal electric field. With the increase of temperature, the movement of the electric dipoles becomes easier and the dipoles move parallel to the ac external electric field and then the internal electric field increased and acts to decrease the dielectric constant [31, 32].

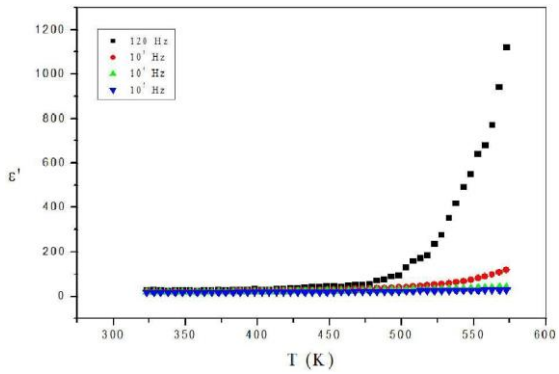

Figure 12. The variation of the dielectric constant versus Temperature at various frequencies, for the sample containing 45 mol% BCD, as representative figure

Fig. (13), shows the variation of the dielectric loss factor (ε″) as a function of temperature for the sample containing 45 mol% BCD, as a representative figure.

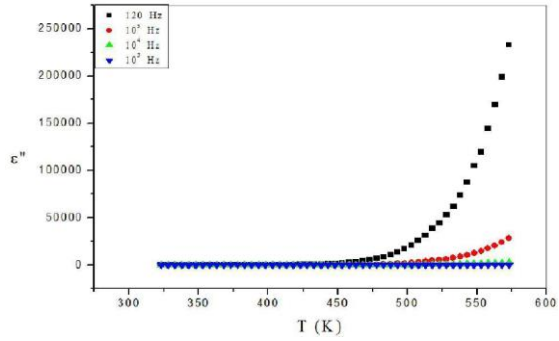

Figure 13. The variation of the dielectric loss factor (ε″) as a function of temperature for the sample containing 45 mol% BCD, as representative figure

It is clear that at low temperatures ε″ exhibit approximately stable value, while at high temperatures it starts to increase as the temperature was increased, and the increment rate is inversely proportional to the frequency. This behavior was explained by Stevels, who divided the energy loss into three parts, the conduction loss, the dipoler loss and the vibrational loss. Since the conduction loss is proportional to σ(ω), therefore ε″ increases as the

conductivity increased, where σ(ω) is temperature dependent quantity [31, 32].

3.4. Gamma-Ray Attenuation parameters

3.4.1. Historical and Theoretical

Until now, the majority of nuclear radiation shields consist mainly of layers of different types of concrete with various compositions and densities as well as layers of lead sheets. But considerable variations of water content in concrete induces high uncertainty factor in calculating their attenuation coefficients due to the continuous variation of their densities, while lead is characterized by its toxicity Moreover, both concert and lead are opaque to visible light [27]. But materials that have to be used for shielding should have stable density and composition as well as they preferable to be transparent. In this regard, glasses are promising materials, since they are usually transparent and easy manufactured.

Berger and Hubbell [34] in 1987 have developed X-COM program for calculating the total mass absorption coefficients or the photon interaction cross-sections for any element, compounds or mixtures at various photon energies from 1 keV to 100 GeV. Recently, X-COM was transformed to the Windows platform by Gerward et al. [35], where it is named Win-XCom. With the development of such program, it becomes easy to calculate the total mass attenuation coefficient for different shielding materials [27, 35, 36].

However, it is preferable to check the ability of the studied glasses to act as transparent shielding materials.

The mass attenuation coefficient can be calculated experimentally by applying the following equation,

$$\mu_m = \ln (I_0 / I) / \rho_x \quad (7)$$

Where ρ_x is the measured experimental density of a material (g/cm^3), I_0 and I are the incident and transmitted intensities respectively, and x is the thickness of the absorber (cm). But the value of the total mass attenuation coefficient of a mixture or compound can be calculated applying Win-X-COM program (based on the mixture rule) by using equation (8) [33],

$$\left(\frac{\mu}{\rho}\right)_m = \sum_i^n w_i \left(\frac{\mu}{\rho}\right)_{mi} \quad (8)$$

where $(\mu/\rho)_m$ is the total mass attenuation coefficient of a sample (mixture or compound), $(\mu/\rho)_{mi}$ is the total mass attenuation coefficient the composing elements of such sample and w_i is the fractional weights of each element in the studied sample. Theoretical values for the total mass attenuation coefficient can be found in the tables prepared by Hubbell and Seltzer [36].

The linear attenuation coefficients (μ_L) can be then calculated and the obtained values are correlated to the half value layer (HVL) according to equation (9),

$$HVL = 0.693/ \mu_L \quad (9)$$

where HVL is the thickness of the material that decreases the intensity of the incident photon to its half value.

The Mean free path (MFP) of a gamma-ray photon (λ), was then calculated by using equation (10),

$$\lambda\ (MFP) = 1/\mu_L \quad (10)$$

where (λ) is the mean distance that the photon can travel between two successive interactions of the photon and matter.

3.4.2. Total mass attenuation coefficient calculations

Fig. (15) shows the variation of the calculated μ_m values for the studied glasses at different low γ-ray energies as a function of BCD content. It was found that μ_m show generally, slight linear increase with the increase of the weight fraction of BCD at the expense of P_2O_5. This may be due to the gradual increase in the density of the investigated glass samples. In addition, the increase in photon interaction probability at these energies leads to the decrease of gamma-rays transmission with the increase in the amount of P_2O_5, which indicates better shielding properties.

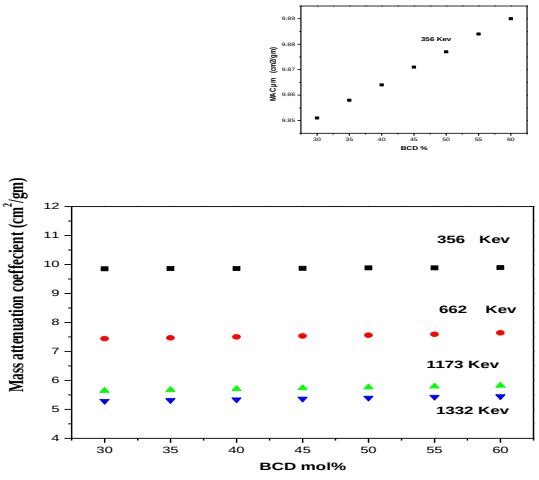

Figure 15. The variation of μ_m as a function of BCD at different low γ – ray energies

The numerical values of the calculated μ_m at different energies are summarized in Table (3).

3.4.3. Linear attenuation coefficient (μ_L) calculations

The linear attenuation coefficient (μ_L) is the fraction attenuated from the incident photons per unit thickness of a material. It represents the fraction of

photons removed from a monoenergetic beam per unit thickness of a material and it is expressed in units of 1/cm.

Fig. (16) shows the variation of linear attenuation coefficient as a function of BCD content, at different low gamma-ray energies. It appeared that, μ_L increases with the increase of BCD, which may be due to the gradual increase of density.

Table 3. The variation of the Mass attenuation coefficient as a function of BCD at relatively low γ–ray energies

Glass No	BCD mol%	Density gm/cm^3	μm (cm^2/gm) X (10^{-2})			
			356 Kev	662 Kev	1173 Kev	1332 Kev
1	30	1.93	9.851	7.44	5.641	5.289
2	35	2.35	9.858	7.471	5.67	5.317
3	40	2.48	9.864	7.502	5.699	5.344
4	45	2.62	9.871	7.532	5.728	5.371
5	50	2.71	9.877	7.563	5.757	5.398
6	55	2.85	9.884	7.593	5.786	5.425
7	60	3.16	9.89	7.64	5.816	5.445

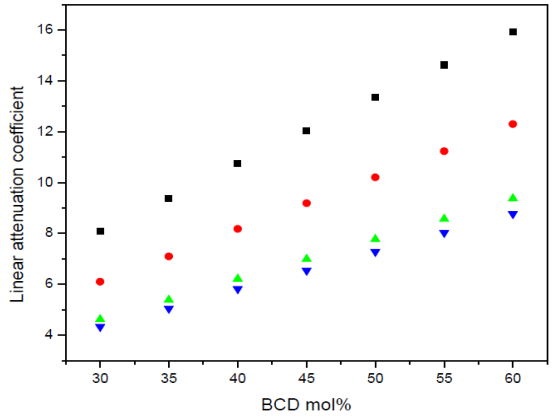

Figure 16. The variation of the μ_L as a function of BCD content at different low γ-ray energies

3.4.3. The half value layer and mean free path calculations

The HVL is the thickness of a material required to reduce the intensity of the transmitted radiation into its half value. Such value can be used to describe the effectiveness of the studied shields.

Fig. (17) shows the behavior of HVL for the studied glasses as a function of BCD, at various low gamma-ray energies. This figure indicates that HVL decreases with the increase of the weight fractions of BCD. This may be due to the gradual increase of linear attenuation coefficient and the densities of the studied glass samples.

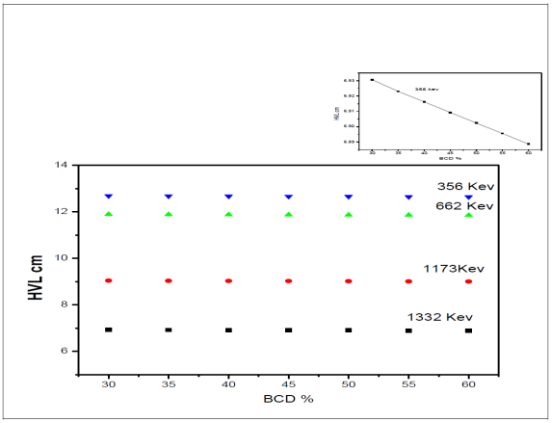

Figure 17. The variation of HVL as a function of BCD at relatively low γ – ray energies

The numerical values of the calculated HVL at different low γ–ray energies are summarized in Table (4).

Table 4. The calculated HVL as a function of BCD, at relatively low gamma-ray energies

Glass No	BCD (mol%)	Density (gm/cm^3)	HVL			
			356 Kev	662 Kev	1173 Kev	1332 Kev
1	30	1.92905	9.999	7.665	5.828	5.462
2	35	2.34899	10.01	7.670	5.831	5.465
3	40	2.47639	10.02	7.675	5.835	5.469
4	45	2.62365	10.03	7.681	5.838	5.472
5	50	2.70551	10.04	7.686	5.842	5.475
6	55	2.85243	10.05	7.691	5.845	5.478
7	60	3.15972	10.06	7.696	5.848	5.481

The MFP is the average distance traveled by a moving photon between successive impacts. Such value can be used to describe the effectiveness of the studied shields. Fig. (18), shows the behavior of the MFP for the studied glasses as a function of BCD, at various low gamma-ray energies. This figure indicates that MFP decreases with the increase of the weight fractions of BCD. This may be due to the gradual increase of molar volume of the studied glass samples.

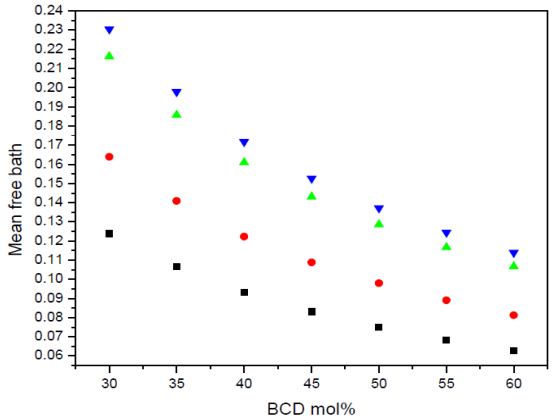

Figure 18. The variation of MFP, as a function of BCD content

and to the gradual increase of μ_L[37].

Noticing that, the studied glasses contained no any heavy metal cations (only phosphorous and BCD constituting cations), and it is supposed that, if some heavy metal cations are introduced into their network, this may improve their gamma-ray attenuation parameters. However, these parameters will be checked now when different amounts of BaO are introduced into their networks.

3.4.4. The Total Mass Attenuation Coefficient of samples containing BaO

The mass attenuation coefficients as a function of γ- ray energies for different BaO concentrations are represented in Table (5) and Fig. (19).

Table 5. The mass attenuation coefficient values of all samples at different γ-ray

	1332	1173	662	356
0.5	0.45	0.4	0.35	30%
1.21E-01	1.19E-01	1.17E-01	1.15E-01	1.13E-01
7.71E-02	7.71E-02	7.71E-02	7.71E-02	7.70E-02
5.57E-02	5.60E-02	5.62E-02	5.65E-02	5.68E-02

It can be observed from Table (5) that the mass attenuation coefficient exhibits approximately gradual increase as BaO was increased, but it shows approximately gradual decrease as the γ- ray energy was increased. This behavior shows good confirmation that the introduced BaO act to increase the mass attenuation coefficient. It appeared also that the studied glass sample exhibit high efficiency at low γ- ray energies and their efficiency decreased as γ- ray increased.

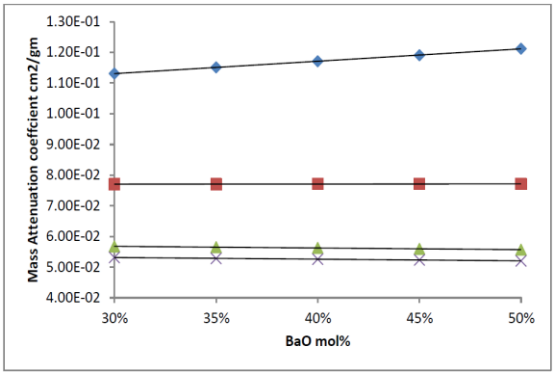

Figure 19. The variation of μ_m of glasses containing different concentration of BaO

Generally, these results indicate that the present glass system is a good attenuator for gamma photons and promising gamma-ray shielding material due to their high mass attenuation coefficient and their low half value layer (HVL), especially when some BaO has introduced into their glass networks.

4. Conclusion

It is possible to recycling BCD in glass manufacture is a matter of interest due the accumulation of huge amounts as well as its dangerous attack to the human reparatory system. It was concluded also that, phosphate glasses accept up to 60 mol% of BCD to give pure transparent and homogenous glasses, which evidenced by comparing the experimental and empirical density and molar volume values as well as by XRD results. It was found, that all glasses behave like semiconductors. The mixed alkali-alkaline earth effect (CaO & K_2O) act to corrupt the expected linear behavior of the total conductivity dependence BCD concentration.

The studied glasses represent good attenuators for γ –photons and promising gamma-ray shielding material due to their high mass attenuation coefficient and their low half value layer (HVL) only at low gamma-ray energies. The introduced of some heavy metal cation improve all the gamma-ray shielding parameters.

Corresponding Author:
Prof. Dr. Ahmed G. Mostafa
Phys. Dept., Faculty of Science
Al-Azhar Univ., Nasr City, Cairo, Egypt
E-mail: drahmedgamal.@yahoo.com

References

1. Y. M. Mustafa and A. AL. Adway, Phys.Status Solid (A),179 (2000) 83.
2. E. Metwalli, M. Karabulut, D. L. Sideborton, M. Mrsi and R.K. Brow, J. Non-Cryst. Sollids, 344 (2004) 128.
3. S. W. Martin, J. Am. Ceram. Socity, 71 (1988) 438.
4. R. Mercier, J. P. Malugani, B. Fahys, and G. Robert, Solid State Ionics, 5 (1981) 663.
5. M. Wada, M. Mcnetrier, A. Le Vasseur and P. Hagenmuller, Mater. Res. Bull., 18 (1983) 189.
6. H. Mori, H. Matsuno and H. Sakata, J. Non-Cryst Solids, 276 (2000) 78.
7. G. D kattak, E. E. Khfaja, L. E. Wenge, D. J. Thompson, M. A. Said, A. B. Hallak and M. A. Daous, J. Non-Cryst. Solids, 194 (1990) 1.
8. A. saeed, R.M. El-Shazly, Y.H. Elbashar, A.M.A. El-Azm and M.M. El-Okr, Radiat. Phys. Chem., 102(2014)167.
9. H.A. Saudi, A. Abd-Elalim, T.Z. Abou-Elnasr, A.G.Mostafa,Nature and Scince,13(11) (2015)139.
10. A.M. El-Khayatt, A. M.Ali and V.P. Singh, Nucl.Inst. Methods Phys. Res. (A),735 (2014) 2014.
11. A. A. Bendary, Ph. D. Thesis, Phys. Dept. Faculty of Science, AL-Azhar Univ., Egypt, (2014).
12. S. Grandi, P. Mustarelli, A. Magistris, M. Gallorini and E. Rizzio, J. Non-Cryst. Solids, 303 (2002) 208.
13. A. Feltri, S. Grandi, P. Mustarelli, M. Cutroni and A. Mandanici, J. Solid State Ionics, 154 – 155 (2002) 217.
14. S. Duhan, S. Sanghi, A. Agarwal, A. Sheoran and S. Rani, Physica B, 404 (2009) 1648.
15. N.T. Sheldon Landsberger, "Measurement & Detection of Radiation" 4th edition, France (2015).
16. A.M. Abdel-Ghany, M.S.S. Saad, I.I. Bashter, T.Z. Amer, S.M. Salem and A.G. Mostafa, Nature and Scince, 12(2014)162.
17. B. Qian Xiaofeng Liang, Shiyuan Yang, Shu He and Long Gao, J. Molecular Structure, 1027 (2012) 31.
18. A. M. Efimov, J. Non- Cryst. Solids, 209 (1997) 209.
19. A. G. shikerkar, J. A. E. Desa, P. S. R. Krishna and R. chitra, J. Non-Cryst. Solids, 270 (2000) 234.
20. J. C. Buyn, B. H. Kim, K. S. Hong, H. J. Jung, S. W. Lee and A. A. Lzyneev, J. Non-Cryst. Solids, 190 (1995) 288.
21. J. Koo, B. S. Bae and H. K. Na, J. Non-Cryst. Solids, 212 (1997) 193.
22. S.W. Martin, Eur. J. Solid Inorg. Chem., 28(1) (1991) 163.
23. L. Baia, D. Muresan, M. Baia, J. Popp and S.Simon, Vib. Spectrosc., 43 (2007) 313.
24. S. N. Salman and H. A. El-Batal, J. Non-Cryst. Solids, 168 (1994) 179.
25. C. Daynand and M. S. Graw, J. Mater. Sci, 31 (1996) 1945.
26. S. Wuy, X. Wei, X. Wang, H. Yang and H. Gao, J. Mater. Sci. & Technol., 26 (5) (2010) 472.
27. P. Muralidharan, M. Venkateshwarlu and N. Satyanarayana, J. Non-Cryst. Solids, 351(2005) 583.
28. A.M. Abdel-Ghany, A.A. Bendary, T.Z. Abou-El-Nasr, M.Y. Hassan and A.G. Moustafa. Nature and Science, 12(2014)126.
29. S. S. Fouad, A. E. Bekheet and A. M. Farid, Physica B, 322 (2002) 163.
30. R. Elliot, Adv. Phys., 18 (1987) 31.
31. A. M. Abdel-Ghany, Ph. D. Thesis, Phys. Dept., Faculty of science AL-Azhar Univ., (2011). .
32. F. M. Ezz Eldin and N. A. El-Alaily, Materials Chem. and Phys., 52(1998) 175.
33. J.F. Krocher, R.E. Browman "Effects of Radiation on Materials and Components", Reinhold, New York, (1984).
34. J. Berger, J.H. Hubbell, NBSIR (1987), 87.
35. L. Gerward, N. Guilbert, K.B. Jensen and H. Levring, Radiat. Phys. Chem., 60 (2001) 23.
36. J.H. Hubbell, S.M. Seltzer, NISTIR 5632 (1995).
37. A.M. Abdel-Ghany, A.M. Zoulfakar,T.Z. Abo-Elnaser, M.Y. Hassan and A.G. Moustafa, American Journal of Phys. and Applications, 3(6) (2015) 208.

12/30/2017